7-28-2023

IFIT2 Restricts Murine coronavirus Spread to the Spinal Cord White Matter and Its Associated Myelin Pathology

Madhav Sharma

Debanjana Chakravarty

Afaq Hussain

Ajay Zalavadia

Amy Burrows

See next page for additional authors

AMERICAN SOCIETY FOR MICROBIOLOGY | Journal of Virology

Virology | Full-Length Text

Ifit2 restricts murine coronavirus spread to the spinal cord white matter and its associated myelin pathology

Madhav Sharma,[1] Debanjana Chakravarty,[1] Afaq Hussain,[1] Ajay Zalavadia,[2] Amy Burrows,[2] Patricia Rayman,[2] Nikhil Sharma,[2] Lawrence C Kenyon,[3] Cornelia Bergmann,[4] Ganes C. Sen,[2] Jayasri Das Sarma[1]

AUTHOR AFFILIATIONS See affiliation list on p. 20.

ABSTRACT Interferon-induced protein with tetratricopeptide repeats 2, Ifit2, is critical in restricting neurotropic murine-β-coronavirus, RSA59 infection. RSA59 intracranial injection of Ifit2-deficient (-/-) compared to wild-type (WT) mice results in impaired acute microglial activation, reduced CX3CR1 expression, limited migration of peripheral lymphocytes into the brain, and impaired virus control followed by severe morbidity and mortality. While the protective role of Ifit2 is established for acute viral encephalitis, less is known about its influence during the chronic demyelinating phase of RSA59 infection. To understand this, RSA59 infected Ifit2$^{-/-}$ and Ifit2$^{+/+}$ (WT) were observed for neuropathological outcomes at day 5 (acute phase) and 30 post-infection (chronic phase). Our study demonstrates that Ifit2 deficiency causes extensive RSA59 spread throughout the spinal cord gray and white matter, associated with impaired CD4^{+} T and CD8^{+} T cell infiltration. Further, the cervical lymph nodes of RSA59 infected Ifit2$^{-/-}$ mice showed reduced activation of CD4^{+} T cells and impaired IFNγ expression during acute encephalomyelitis. Interestingly, BBB integrity was better preserved in Ifit2$^{-/-}$ mice, as evidenced by tight junction protein Claudin-5 and adapter protein ZO-1 expression surrounding the meninges and blood vessels and decreased Texas red dye uptake, which may be responsible for reduced leukocyte infiltration. In contrast to sparse myelin loss in WT mice, the chronic disease phase in Ifit2$^{-/-}$ mice was associated with severe demyelination and persistent viral load, even at low inoculation doses. Overall, our study highlights that Ifit2 provides antiviral functions by promoting acute neuroinflammation and thereby aiding virus control and limiting severe chronic demyelination.

IMPORTANCE Interferons execute their function by inducing specific genes collectively termed as interferon-stimulated genes (ISGs), among which interferon-induced protein with tetratricopeptide repeats 2, Ifit2, is known for restricting neurotropic viral replication and spread. However, little is known about its role in viral spread to the spinal cord and its associated myelin pathology. Toward this, our study using a neurotropic murine β-coronavirus and Ifit2-deficient mice demonstrates that Ifit2 deficiency causes extensive viral spread throughout the gray and white matter of the spinal cord accompanied by impaired microglial activation and T cell infiltration. Furthermore, infected Ifit2-deficient mice showed impaired activation of T cells in the cervical lymph node and relatively intact blood–brain barrier integrity. Overall, Ifit2 plays a crucial role in mounting host immunity against neurotropic murine coronavirus in the acute phase while preventing mice from developing viral-induced severe chronic neuroinflammatory demyelination, the characteristic feature of human neurological disease multiple sclerosis (MS).

KEYWORDS Ifit2, coronavirus, demyelination, microglia, interferon-gamma

The immunomodulatory properties of interferons (IFNs) make them useful in the treatment of multiple sclerosis (MS), which is a chronic inflammatory

Editor Tom Gallagher, Loyola University Chicago, Maywood, Illinois, USA

Address correspondence to Jayasri Das Sarma, dassarmaj@iiserkol.ac.in.

Cornelia Bergmann and Ganes C. Sen are joint senior authors.

The authors declare no conflict of interest.

See the funding table on p. 20.

Received 31 May 2023
Accepted 11 June 2023
Published 28 July 2023

neurodegenerative demyelinating disease of the central nervous system (CNS) (1–4). The action of IFNs is mediated by the expression of numerous genes called IFN-stimulated genes (ISGs) that encode for antiviral and immunomodulatory factors (5). Among these, IFN-induced protein with tetratricopeptide repeat 2 (Ifit2) is a restriction factor against rabies virus, vesicular stomatitis virus, West Nile virus, Sendai virus, murine β-coronavirus, and mouse hepatitis virus (MHV) (6). Several studies, including those with MHV, have explored the underlying antiviral regulatory mechanisms of Ifit2 (6, 7). Neurotropic strain of murine β-coronavirus induces acute encephalomyelitis and meningitis followed by chronic progressive demyelination upon intranasal as well as intracranial administration (8, 9). However, previous studies have shown that intracranial inoculation of the virus is a more reliable and potent way to understand the neurological manifestation of MHV-induced demyelinating disease (10).

Intracranial infection with the demyelinating strain MHV-A59 or its spike protein isogenic recombinant strain RSA59 in mice initiates activation of innate immune responses followed by prominent adaptive immunity, which controls virus replication and drops infectious virus titers below the detection limit by day 15 post-infection (p.i.). However, viral RNA persists at a very low level. A gradual increase in myelin pathology with or without axonal loss is evident as early as day 7 p.i. and reaches its peak during the persisting phase (day 30 p.i.), mimicking certain pathological features of human neurological demyelinating disease, multiple sclerosis (11–15). Intracranial inoculation of Ifit2$^{-/-}$ mice with low doses of RSA59, which otherwise elicits only mild symptoms in wild-type (WT) mice, caused pronounced morbidity and mortality, accompanied by uncontrolled virus replication with significantly impaired microglial activation, reduced expression of CX3CR1, and reduced recruitment of NK1.1^{+} and CD4^{+} T cells into the brain (7).

While the role of Ifit2 in acute inflammation is well-established, the impact of Ifit2 deficiency on virus spread to the spinal cord and its associated neuroinflammatory demyelination remains to be investigated. The current study reveals significantly heightened, indiscriminate viral spread within spinal cord gray and white matter, fewer Iba1^{+} microglia/macrophages, and impaired local T cell infiltration in Ifit2$^{-/-}$ spinal cords, similar to that observed in the brains during acute infection. Viral antigen persisted prominently during chronic disease relative to its sparse detection in WT spinal cords. Reduced activation of CD4^{+} T cells in draining cervical lymph nodes (CLNs) was consistent with the inability of the immune system to clear infectious viruses from the CNS. Furthermore, blood–brain barrier (BBB) integrity was maintained in Ifit2$^{-/-}$ compared to WT mice despite elevated virus load. Although Ifit2$^{-/-}$ mice given a comparatively low dose of RSA59 survived, they developed severe progressive clinical symptoms associated with augmented white matter demyelination and gray matter pallor, compared to sparse demyelination not affecting the gray matter in WT mice. Demyelinated lesions in Ifit2$^{-/-}$ mice exhibited significantly more ameboid phagocytic microglia/macrophages. Overall, our data suggest that lack of Ifit2 reduces the immune cell priming in CLN and, preserves BBB integrity, thereby leading to reduced infiltration into the CNS at the acute phase. This allows enhanced virus replication throughout the chronic phase of neuroinflammation, promoting microglia/macrophage phagocytosis and leading to detrimental chronic demyelination.

RESULTS

Ifit2 deficiency significantly increased RSA59 spread but restricted microglial activation in the spinal cords at the acute phase of neuroinflammation

Inoculation of WT mice with RSA59 into the brain near the lateral geniculate nuclei results in rapid viral spread to the olfactory bulb, cerebral cortex, ventral striatum/basal forebrain, hippocampal region, midbrain, and medulla, followed by infection of the brainstem and deep cerebellar white matter and ultimately, the spinal cord white matter indicated by histopathological analysis of brain and spinal cord (11). Previous studies showed that Ifit2 played a significant antiviral role against RSA59 dissemination

within the brain in 4–5-week-old mice even at inoculation doses of 2000 PFUs, which is one-tenth of half of the LD50 dose. Ifit2$^{-/-}$ mice developed severe clinical distress and hind limb paralysis compared to WT mice and succumbed to infection by day 8 p.i (7). In the current study, RSA59 replicates profusely throughout the spinal cord gray and white matter in Ifit2$^{-/-}$ mice (Fig. 1A and B). In contrast, viral spread in RSA59-infected WT mice was mainly contained to the white matter of the dorsal columns with minimal spillover into the gray matter as shown by immunohistochemical detection of nucleocapsid protein at day 5 p.i., representing the enhanced virus replication (Fig. 1A and C). In contrast to the profuse viral spread, microglial activation was significantly impaired in RSA59-infected Ifit2$^{-/-}$ spinal cords, as evidenced by limited expression of ionized calcium-binding adaptor molecule 1 (Iba1), which marks microglia/macrophages, at day 5 p.i. (Fig. 1D through F). No significant differences were observed in astrocytic glial fibrillary acidic protein (GFAP) expression in the spinal cords of RSA59-infected Ifit2$^{-/-}$ compared to WT mice (Fig. 1G through I). Thus, Ifit2 deficiency restricts microglial/macrophage activation throughout the CNS upon acute RSA59 infection.

Ifit2 deficiency reduces lymphocyte infiltration in RSA59-infected acutely inflamed spinal cords

Neutrophils are the first leukocytes to enter the brain of RSA59-infected mice, followed by circulating monocytes and T lymphocytes (7, 16). Flow cytometric analysis of spinal cord cells was performed to assess differences in the infiltration of specific leukocyte populations in RSA59-infected WT versus Ifit2$^{-/-}$ mice at days 3, 5, and 7 p.i. Gating on total CD45^{+} cells allowed distinction between CD45$^{lo/in}$ microglia and CD45^{hi} peripheral infiltrating leukocytes. The CD45^{hi} population increased markedly at days 5 and 7 p.i. in WT and Ifit2$^{-/-}$-infected mice (Fig. 2A and B). However, CD45^{hi} cells were significantly reduced in Ifit2$^{-/-}$-infected mice compared to WT-infected mice at day 7 p.i. (Fig. 2C). To assess whether reduced leukocyte recruitment to the spinal cord involved a specific cell type, we monitored early infiltrating CD45^{hi} cells via immunophenotyping. Spinal cord-derived cells were assessed for CD4^{+} T and CD8^{+} T cell subsets (Fig. 2D). The number of CD4^{+} T cells increased between day 5 to 7 p.i. in the spinal cord of WT mice and from day 3 to 5 as well as from day 5 to 7 p.i. in Ifit2$^{-/-}$ mice (Fig. 2E). Infiltrating CD8^{+} T cells increased between both day 3 to 5 and day 5 to 7 p.i. in WT as well as Ifit2$^{-/-}$ mice (Fig. 2G). Both WT and Ifit2$^{-/-}$ spinal cords harbored similar lymphocyte cell numbers at days 3 and 5 p.i.; however, there were significantly fewer CD4^{+} T and CD8^{+} T cells in the spinal cord of Ifit2$^{-/-}$ compared to WT mice at day 7 p.i. (Fig. 2F and H). Staining for Ly6G to mark neutrophils revealed a significant reduction from day 3 to 5 in WT mice; however, no change was observed between the groups throughout days 3 to 7 p.i. (Fig. 2I through K). A previous study using MHV demonstrated that CD4^{+} T cell interaction with microglia/macrophages is required for effective viral antigen clearance and maintenance of CNS homeostasis (16). Thus, impaired CD4^{+} T cell and microglia/macrophage communication may underlie the disease severity in Ifit2$^{-/-}$ mice.

Ifit2 deficiency impaired expression of selected cytokine and chemokine in CNS and CLN upon RSA59 acute infection

Neurotropic MHV infection in WT mice upregulates genes involved in host innate immune response such as IFNs and their induced genes, guanylate-binding proteins (GBPs), GTPases, cytokines, and chemokines associated with activation of peripheral as well as CNS resident immune cells (14). These genes also play an important role in BBB regulation, cytoskeleton reorganization, antigen presentation, cell adhesion, and immune cell migration in CNS. Previous studies using Ifit2$^{-/-}$ mice infected with MHV have shown impaired expression of IFNα, IFNβ at day 3 and 5 p.i. in the CNS with temperate alteration in the expression of IFNγ, IL-6, CCL2, CCL5, CSF2, CXCL9, CXCL10, and Nos2 at day 3, 5, and 7 p.i. as compared to the WT mice (7, 17). Our data using qPCR indicate that mRNA expression of BBB-destabilizing cytokines such as IL-1β and TNFα were similar in Ifit2$^{-/-}$ and WT mice (Fig. 3A and B).

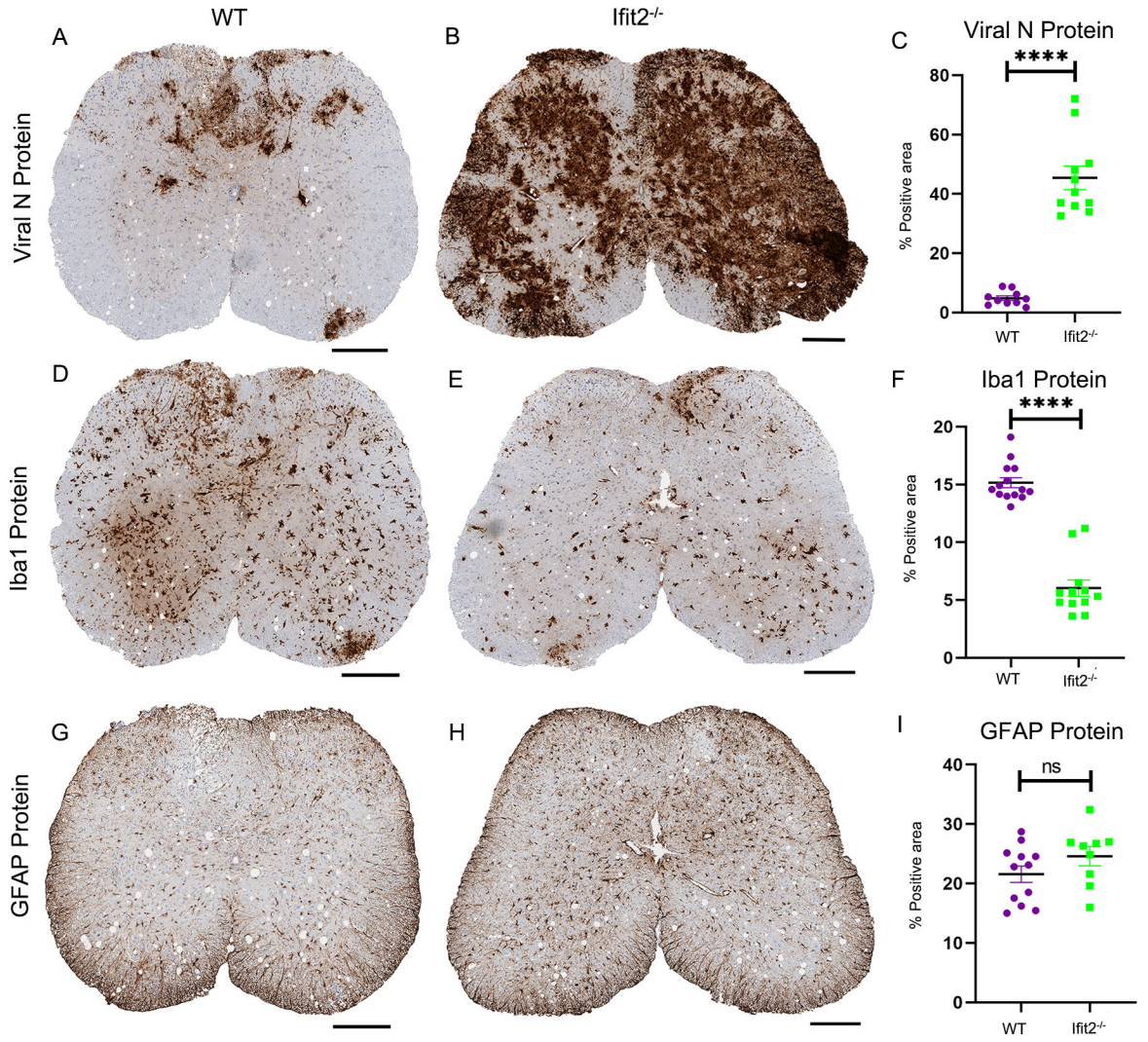

FIG 1 Ifit2 deficiency increases virus spread but restricts microglial activation in RSA59-infected spinal cords during acute infection. 5 µm thick serial sections from spinal cord tissues at day 5 p.i. were stained for viral nucleocapsid protein (A and B), Iba1 for microglia/monocyte/macrophages (D and E), and GFAP for astrocytes (G and H). The scale bar is 200 µm. Quantification of viral N protein, Iba1, and GFAP expression is graphically represented in panels C, F, and I, respectively. The experiment was repeated three times with four to five mice per experiment. Purple color in graphical representation denotes WT and green color denotes Ifit2$^{-/-}$ mice. Each dot represents an average of multiple section of single animal. Asterix (*) represents differences that are statistically significant by Student's unpaired *t*-test analysis (*$P < 0.05$, **$P < 0.01$, ****$P < 0.0001$). The error bars represent SEM.

CLNs are the secondary lymphoid organs present near the cervical region of the spinal cord and are known for their essential role in activating adaptive immune responses against various neurotropic viruses. mRNA expression of selected cytokines and chemokines was analyzed at day 5 p.i., considering the fact that activated T cells start to infiltrate the CNS from day 5 p.i., to counter the viral replication and spread (7, 16). CLN mRNA expression of IFN-α and IFN-β remained unaltered at day 5 p.i. in RSA59-infected Ifit2$^{-/-}$ and WT mice (Fig. 3C and D). However, mRNA expression of IFNγ, which enhances antigen presentation in APCs, thus modulating the innate immune response toward a more antigen-specific response, was significantly lower in Ifit2$^{-/-}$ compared to WT mice (Fig. 3E). mRNA analysis of viral N gene revealed the presence of enhanced viral load in CLN of Ifit2$^{-/-}$ as compared to WT mice (Fig. 3F), whereas mRNA expression of CXCL9, CD4, CD8, CSF2, CD40 was significantly reduced (Fig. 3G through 3K). Overall, the mRNA data indicate that despite higher viral loads in CLN the expression of various

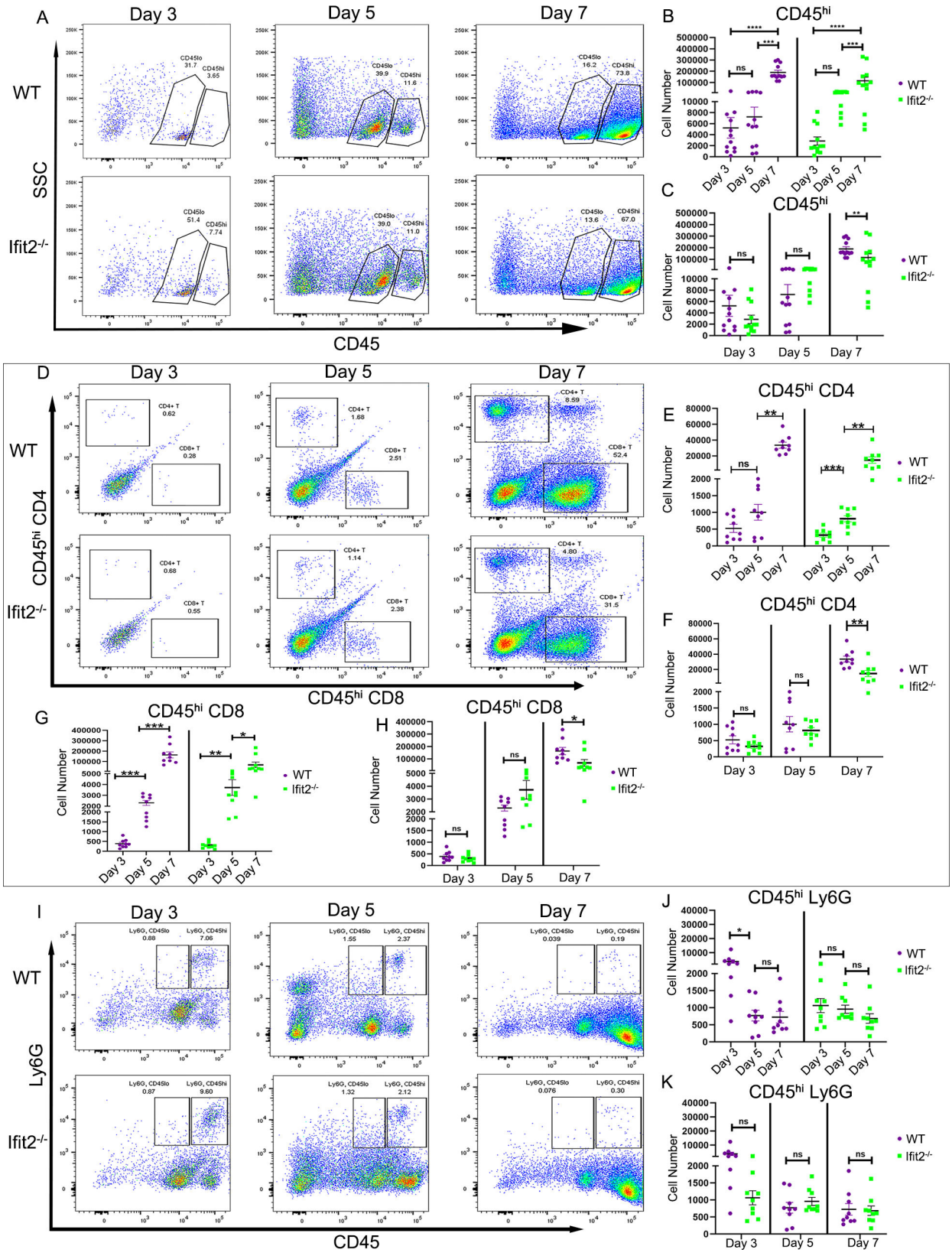

FIG 2 Ifit2 deficiency reduces T cell infiltration into RSA59-infected spinal cord. Spinal cords from infected WT and Ifit2$^{-/-}$ mice were harvested at days 3, 5, and 7 p.i. for flow cytometric analysis. Dot plots represents stains at days 3, 5, and 7 p.i. gated on total live cells and showing CD45^{LO} and CD45^{HI} cells (panel A), CD4 and CD8 cells gated on CD45^{HI} cells (panel D), and Ly6G-expressing cells in the CD45^{HI} gate (panel I). Absolute numbers of CD45^{HI}, CD45^{HI}CD4^{+}, CD45^{hi}CD8^{+}, and

(Continued on next page)

FIG 2 (Continued)

$CD45^{HI}Ly6G^{+}$ cells recovered from WT and $Ifit2^{-/-}$ spinal cords at indicated timepoints are compared within each group across timepoints (B, E, G, J) and between WT and $Ifit2^{-/-}$ mice at each timepoint (C, F, H, K) as indicated. Purple color in the graphical representation denotes WT and green color denotes $Ifit2^{-/-}$ mice. The data were pooled from three to four independent experiments with n = 9–12. Each dot represents a single animal. Asterix (*) represents differences that are statistically significant by Student's unpaired t-test analysis (*$P < 0.05$, **$P < 0.01$, ****$P < 0.0001$). The error bars represent SEM.

inflammatory cytokines/chemokines was impaired, suggesting an inability to mount a host immune response to clear the virus in $Ifit2^{-/-}$ as compared to WT mice.

Ifit2 deficiency impaired $CD4^{+}$ T cell activation, and IFNγ production in the CLN upon RSA59 acute infection

Upon activation in CLN, T cells undergo rapid proliferation and differentiate into effectors capable of migrating to the sites of infection and producing antimicrobial lymphokines (18). IFNγ secreted by T cells plays a critical role in amplifying antigen presentation and recognition via cognate T cell–APC interaction (19). To trace the cause of diminished $CD4^{+}$ T as well as $CD8^{+}$ T cell infiltration into the CNS on day 7 p.i., we assessed the activation of $CD4^{+}$ T cells in the CLN of RSA59-infected WT and $Ifit2^{-/-}$ mice by flow cytometric analysis of activation markers and intracellular staining for IFNγ following nonspecific PMA/IO stimulation *ex vivo*.

CLN of RSA59-infected $Ifit2^{-/-}$ mice compared to WT mice showed reduced population of $CD4^{+}$ T cells (Fig. 4A through E). This reduced $CD4^{+}$ T cell population is accompanied with low production of IFNγ by $Ifit2^{-/-}$ $CD4^{+}$ T cells following *ex vivo* stimulation (Fig. 4F through K). Activation of T cells is marked by specific molecular signatures, including CD44 and CD62L expression (20). Overall, naïve T cells are characterized by their $CD62L^{+}$ $CD44^{-}$, effector/effector memory (EM) cells by their $CD62L^{-}CD44^{+}$, and central memory (CM) cells by their $CD62L^{+}$ $CD44^{+}$ phenotypes, respectively. Reduced numbers of effector/EM $CD4^{+}$ T and $CD8^{+}$ T cells along with increased number of naïve in $Ifit2^{-/-}$ compared to WT mice indicate that Ifit2 deficiency causes impaired activation of T cells (Fig. 4L through X). Overall, these results suggest that Ifit2 deficiency reduces T cell activation and proliferation in the CLN and impairs IFNγ production, which may contribute to their reduced migration to the brain (7) as well as the spinal cord.

Ifit2 deficiency is associated with retention of BBB integrity upon RSA59 infection

The BBB maintains control of CNS homeostasis, protecting the neural tissue from toxins and pathogens. Disruption of these barrier functions can enhance infiltration of peripheral leukocytes into the CNS, thereby promoting control of pathogens, but at the same time resulting in the progression of several neurological diseases (16, 21, 22). To assess if reduced lymphocyte infiltration is associated with preserved BBB integrity, we evaluated BBB permeability using intraperitoneal or intravenous injection of the fluorescent dye Texas red dextran (23) at day 5 post RSA59 infection or mock infection. Examination of fluorescence in the brains of mock-infected control mice demonstrated no difference (Fig. 5A). However, dye injection into infected mice revealed a significantly lower absolute fluorescence in $Ifit2^{-/-}$ relative to WT brain lysates, indicating retention of BBB function in $Ifit2^{-/-}$ compared to WT mice (Fig. 5A through C). To further confirm that Ifit2 deficiency is accompanied by a relatively intact BBB compared to WT mice, we also stained brain sections for claudin-5, a tight junction protein, and the ZO-1 adaptor protein abundantly found in the BBB (24). ZO-1 and claudin-5 were abundantly expressed in $Ifit2^{-/-}$ (Fig. 5G through I) compared to WT mice (Fig. 5D through F). Quantification of the overlapping area (indicated by arrows) between ZO-1 (Red) and claudin-5 (Green) within the total stained area revealed elevated colocalization in the absence of Ifit2 (Fig. 5J). Both the Texas red dextran transmigration assay and more colocalized expression of ZO-1 and claudin-5 indicate that RSA59-infected $Ifit2^{-/-}$ mice have a relatively intact BBB compared to WT mice, implying that Ifit2 promotes BBB

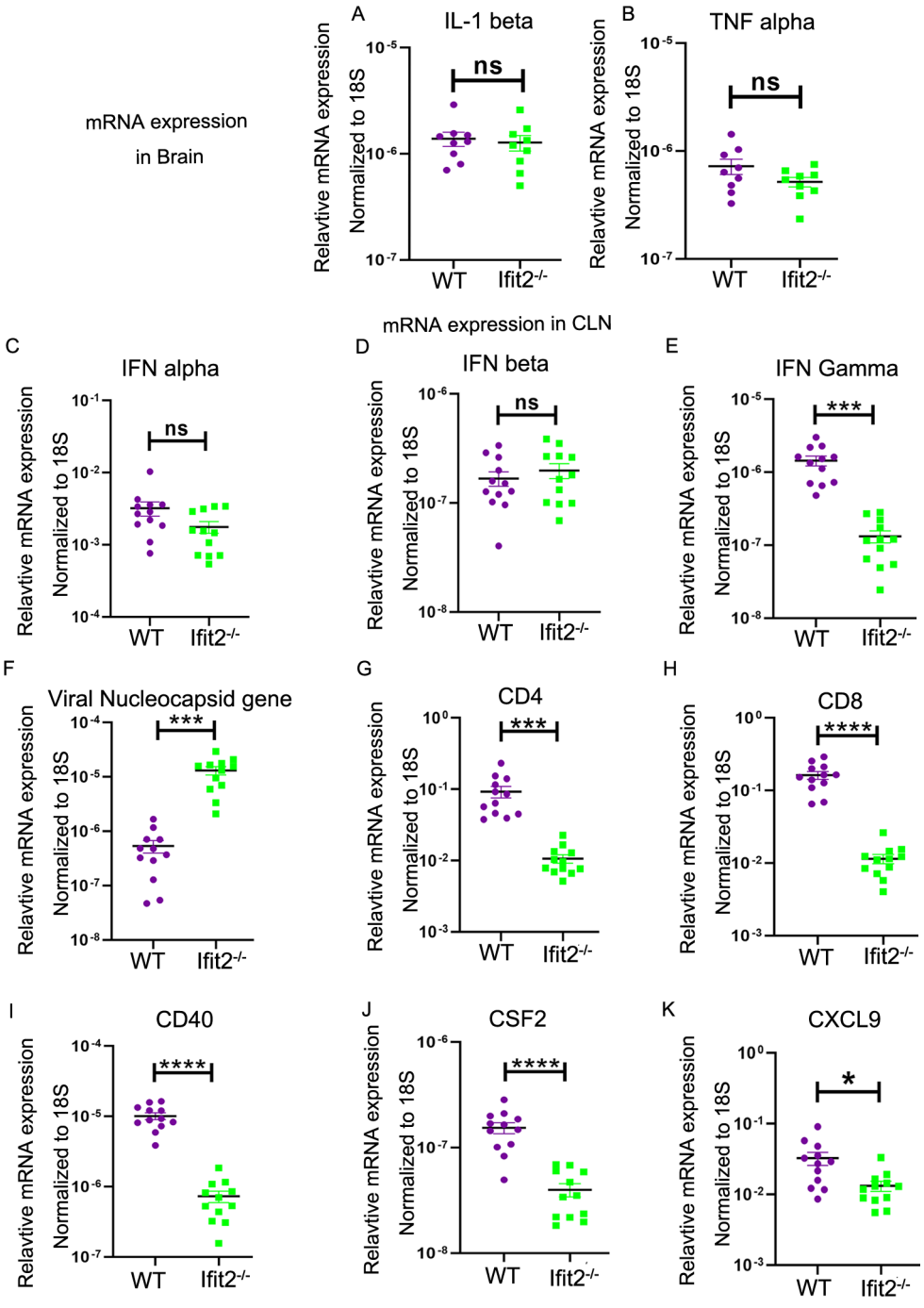

FIG 3 Differential mRNA expression of selected cytokines and chemokines in brains and cervical lymph node (CLN) upon RSA59 acute infection. mRNA extracted from individual brains and CLNs of RSA59-infected WT (purple symbols) and Ifit2$^{-/-}$ mice (green symbols) at day 5 were analyzed for mRNA levels of the indicated cytokines and chemokines by real-time PCR. (A and B) Expression levels of IL-1β and TNF-α mRNA in brains. (C–K) Expression levels of indicated mRNA in CLN. Solid lines represent the mean mRNA expression levels (N = 8–10). Asterix (*) represents differences that are statistically significant by Student's unpaired t-test analysis (*P < 0.05, **P < 0.01, ***P < 0.001, ****P < 0.0001). The error bars represent SEM.

permeability, which allows peripheral immune cell infiltration. The combinatorial effects of reduced T cell priming, impaired IFNγ production in the CLN, and tightened BBB function may thus contribute to insufficient T cell migration to mediate viral control during acute infection.

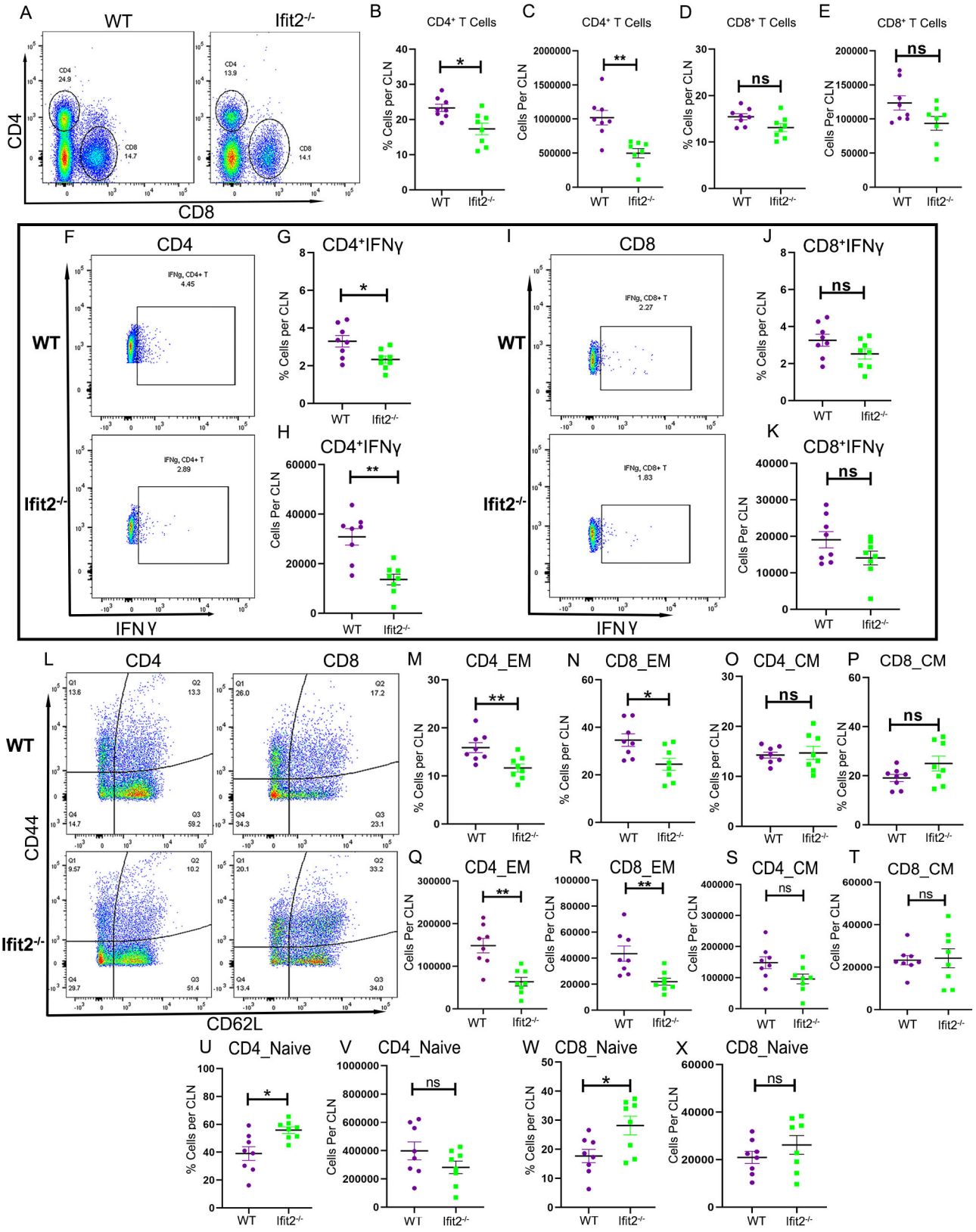

FIG 4 Ifit2 deficiency impairs T cell activation and IFNγ production in cervical lymph nodes (CLN) upon RSA59 acute infection. CLN-derived cells from WT (purple symbols) and Ifit2$^{-/-}$ (green symbols) from RSA59-infected mice were analyzed by flow cytometry for CD4, CD8, CD44, CD62L, and IFNγ expression at 5 days p.i. IFNγ expression was assessed by intracellular staining after 6 h *ex vivo* stimulation with PMA/IO. (A) Representative dot plots showing gating and percentages of

(Continued on next page)

FIG 4 (Continued)

$CD45^{HI}$ $CD4^+$ T and $CD45^{HI}$ $CD8^+$ T cells as indicated. Graphs depict relative percentages and absolute numbers of $CD45^{HI}CD4^+$ (B and C) and $CD45^{HI}$ $CD8^+$ T cells (D and E) in the CLN as indicated. (F and I) Representative dot plots of IFNγ producing cells in CLN-derived $CD45^{HI}$ $CD4^+$ and $CD45^{HI}$ $CD8^+$ T cells. Percentages and absolute numbers of IFNγ producing $CD45^{HI}CD4^+$ (G and H) and $CD45^{HI}$ $CD8^+$ T cells (J and K) in CLN from individual mice. (L) Representative dot plots showing expression of CD62L and CD44 gated on CLN-derived $CD4^+$ or $CD8^+$ T cells from WT and Ifit2$^{-/-}$ mice. (M and N) Percentage of effector/effector memory (EM) T cells marked by their $CD62L^{lo}CD44^+$ expression within the CD4 and CD8 population, respectively. (Q and R) Absolute numbers of effector/effector memory (EM) $CD4^+$ $CD62L^{lo}CD44^+$ and $CD8^+$ $CD62L^{lo}CD44^+$ T, respectively. (O and P) Percentage of central memory (CM) T cells marked by their $CD62L^{hi}CD44^+$ expression within the CD4 and CD8 population, respectively. (S and T) Absolute numbers of CLN-derived CM CD4 and CD8 T cells, respectively. (U,W) Percentage of naïve T cells marked by their $CD62L^{HI}CD44^{LO}$ expression within the CD4 and CD8 population, respectively. (V and X) Absolute numbers of CLN-derived naïve CD4 and CD8 T cells, respectively. The data were pooled from three to four independent experiments with total $N = 8$. Each dot represents a single animal. Asterix (*) represents differences that are statistically significant by Student's unpaired *t*-test analysis (*$P < 0.05$, **$P < 0.01$). The error bars represent SEM.

Ifit2$^{-/-}$ mice exhibit severe demyelination pathology even at 500 PFU of RSA59 infection

Demyelination is the primary characteristic of the human neurological disease, MS. MHV-induced demyelination has provided a model to dissect inflammatory and molecular mechanisms of viral-induced demyelination (1, 11, 13). Given the high mortality of Ifit2$^{-/-}$ mice infected with 2000 PFUs of RSA59, we reduced the virus inoculum in Ifit2$^{-/-}$ mice to 500 PFUs for analysis of demyelinating pathology associated with the persistent phase of infection. The inoculum was maintained at 20,000 PFUs in WT mice as they only developed mild disease symptoms. All Ifit2$^{-/-}$ mice survived until day 30 p.i. with clinical score ranging between 2 and 3, signified by partial to complete hind limb paralysis and severe weight loss (Fig. 6A and B). Spinal cord sections were examined by histopathological analysis at day 30 p.i. Analysis of viral antigen by anti-nucleocapsid (anti-N) immunohistochemistry revealed readily detectable areas of viral persistence until day 30 p.i. in Ifit2$^{-/-}$ mice (Fig. 6D and E). This was in stark contrast to WT mice showing sparse if any anti-N staining reactivity (Fig. 6C through E).

To further understand the viral persistence in white matter region, immunofluorescence was performed using anti-myelin basic protein (MBP), anti-myelin proteolipid protein (PLP), and anti-N antibodies as markers to detect myelin and viral persistence. Immunofluorescence data indicate that Ifit2$^{-/-}$ mice harbor viral antigen till day 30 p.i. in MBP- (6G, arrows) and PLP-stained regions (6I, arrows) in the white matter as opposed to the rare presence of viral antigen in WT mice in MBP- (6F, arrows) and PLP-stained regions (6 H, arrows). These results confirm previously established findings that infectious virus is undetectable by day 30 p.i. in WT mice (1, 13). However, the presence of viral antigen in white matter regions of Ifit2$^{-/-}$ mice even at day 30 p.i. reiterates the inability of the immune system to clear the infectious virus.

Viral persistence in Ifit2$^{-/-}$ mice is correlated with the presence of inflammatory lesions in the spinal cord indicated by H&E staining (Fig. 7A and B). Furthermore, along with more severe myelin loss in the white matter of Ifit2$^{-/-}$ mice (Fig. 7D and E) as compared to WT mice (Fig. 7C and E), corresponding sections stained for microglia/macrophages marker $CD11b^+$ (25) showed that inflammation was primarily resolved in the gray matter of WT mice spinal cords with only a few activated/phagocytic microglia/macrophages present in white matter demyelinated lesions (Fig. 7F). In contrast, Ifit2$^{-/-}$ mice displayed a significantly larger number of $CD11b^+$ immunoreactive cells in both the spinal cord gray and white matter (Fig. 7G and H). Overall, these results indicate that viral antigen persistence in Ifit2$^{-/-}$ mice is associated with severe demyelination and increased $CD11b^+$ myeloid cell reactivity in lesions.

Microglia/macrophages in lesions of Ifit2$^{-/-}$ mice exhibit engulfment of myelin similar to WT mice

To validate that phagocytic microglia/macrophages take up myelin in both WT and Ifit2$^{-/-}$ mice, spinal cords of MHV-RSA59-infected mice were analyzed at day 30 p.i. by confocal immunofluorescence following double immunolabeling for Iba1 and MBP or Iba1 and

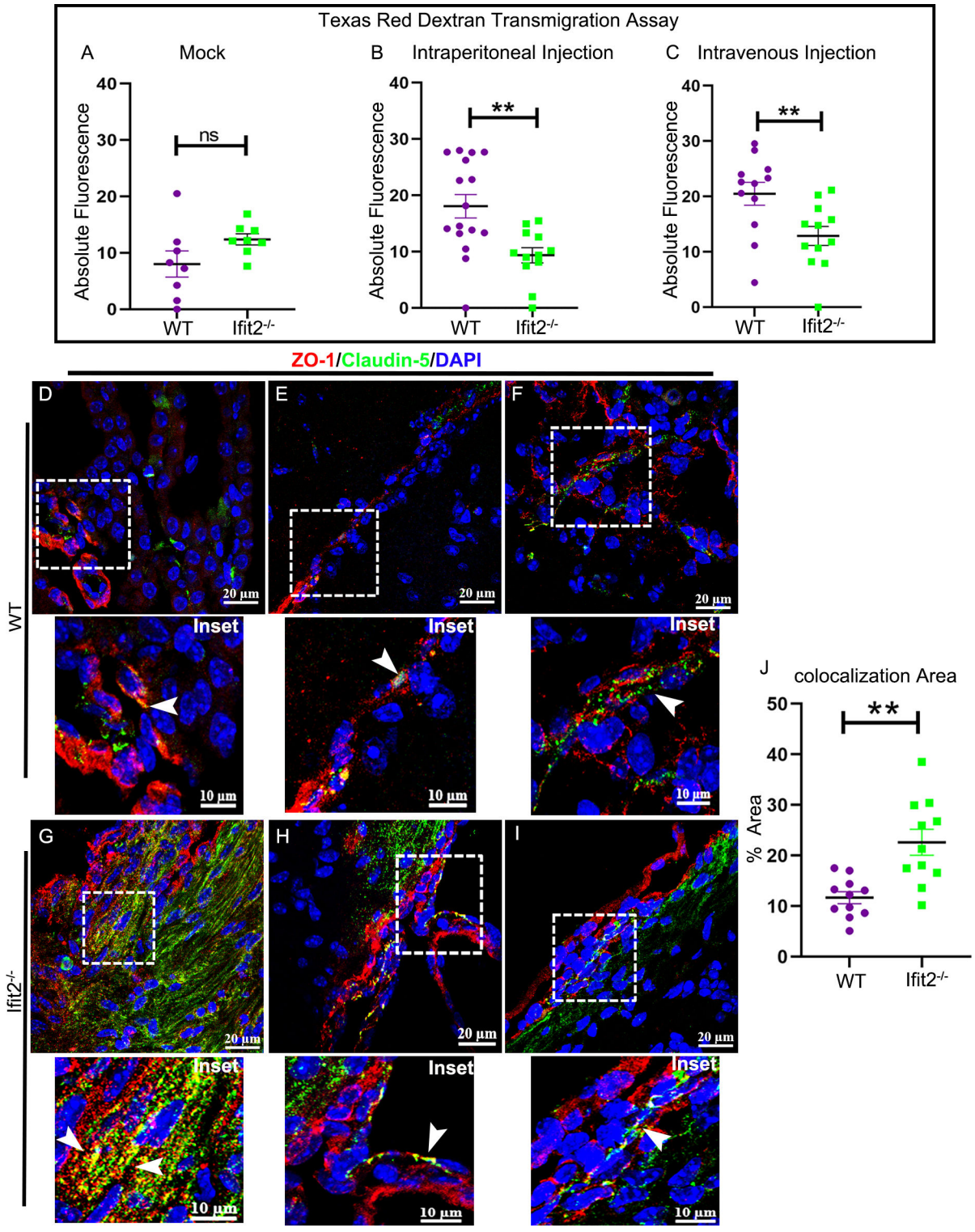

FIG 5 Ifit2 deficiency retained BBB integrity within the brains of RSA59 infected at day 5 p.i. BBB permeability was measured in infected mice following injection of Texas red dextran dye via the IP or IV route at day 5 p.i. Mice mock-infected with PBS and injected IP with dye 5 d later served as controls. Absolute fluorescence of Texas red dextran in brain lysates measured 15 mins post dye injection in control (A) and infected mice as indicated (B, C). 5–10 µm thick paraffin sections were prepared from brains of 4–5-week-old WT and Ifit2$^{-/-}$-infected mice at day 5 p.i. Sections were stained for ZO-1 (red), claudin-5 (green), and nuclei using DAPI (blue). Representative fluorescent images are shown from different regions of the brain such as olfactory region, brain parenchyma, and meninges junction and around blood vessel in WT (D–F, inset indicates enlarged area) and Ifit2$^{-/-}$ mice (G–I, inset indicates enlarged area). Arrowheads indicate ZO-1 and

(Continued on next page)

FIG 5 (Continued)

claudin-5 colocalization staining around the blood vessels and meninges. (J) Quantitative assessment of areas showing colocalization of claudin-5 and ZO-1 out of total stained area excluding DAPI. The experiment was repeated three times with $N = 3$ per experiment. Purple color denotes WT and green color denotes Ifit2$^{-/-}$ mice. Each dot represents a single animal. Asterix (*) represents differences that are statistically significant by Student's unpaired *t*-test analysis (*$P < 0.05$, **$P < 0.01$). The error bars represent SEM.

PLP. MBP and PLP are myelin protein expressed by mature myelinating oligodendrocytes, whereas ionized calcium-binding adaptor molecule 1 (Iba1) marks microglia/macrophages (20, 25, 26). Demyelinated lesions characterized by loss of MBP and PLP staining showed the presence of amoeboid phagocytotic Iba1$^+$ microglia/macrophages in both WT (Fig. 8A and C) and Ifit2$^{-/-}$ mice (Fig. 8B and D). Engulfment of myelin proteins is indicated by areas showing staining overlap between Iba1 and PLP or MBP, respectively (Fig. 8A through D, highlighted by a dashed box). These data indicate that Ifit2$^{-/-}$ myeloid cells are capable of phagocytosing myelin debris despite the apparent limited ability to respond to the acutely replicating virus during early infection. The greater area of myelin loss in Ifit2$^{-/-}$ relative to WT mice (see Fig. 7C through E) is thus associated with elevated viral antigen load and a large number of ameboid-shaped phagocytic microglia/macrophages.

DISCUSSION

IFNs are an integral part of the innate antiviral immune response. IFNs exert their actions by inducing the transcription and translation of a set of genes called IFN-induced genes (ISGs), among which ISG54/Ifit2 plays a crucial role in countering viral replication and dissemination throughout the CNS and peripheral organs (5, 6). Ifit2 contains tetratricopeptide repeats in its structure that facilitate binding with other cellular/viral proteins and RNA molecules (27, 28). Ifit2 is associated with various functions, including antiviral activity, antitumor effects, cell migration, and proapoptotic functions (29–35). Its ability to associate with microtubules further implicates the regulation of microtubule dynamics, cell proliferation, and virion assembly/transport (36). These pleiotropic effects of Ifit2 have made it challenging to elucidate mechanisms underlying its antiviral and protective role *in vivo*.

RSA59 infection of Ifit2$^{-/-}$ mice is associated with enhanced viral load, impaired microglial activation, and restricted CD4$^+$ T cell migration into the brain, despite largely unaltered cytokine and chemokine production; however, the underlying mechanisms remain to be answered (7). Two main checkpoints regulating lymphocyte migration into the CNS are the priming/activation of T cells in secondary lymphoid organs, and the BBB (37, 38). Our study revealed that the CLN of infected Ifit2$^{-/-}$ mice has significantly reduced mRNA expression of immunomodulatory molecules such as IFNγ, CXCL9, CD4, CD8, CSF2, and CD40 with moderate changes in IFNα and IFNβ, despite extensively higher mRNA expression of viral nucleocapsid gene. Impaired IFNγ production in the CLN may thus contribute to ineffective viral control. Furthermore, CLN of infected Ifit2$^{-/-}$ mice has significantly reduced numbers of total as well as IFNγ$^+$ CD4$^+$ T cells compared to WT mice, supporting impaired virus-specific adaptive immune responses. CD4$^+$ T cells are also known to promote the antiviral functions of CD8$^+$ T cells and humoral immunity, both of which contribute to virus control, thus limiting development of severe MHV-induced demyelination (39, 40). Reduced activation of CD4$^+$ T cells in CLN of infected Ifit2$^{-/-}$ mice is confirmed by a significant reduction in effector/EM CD62L^{lo}CD44$^+$ T cells, which supports a role of Ifit2 in the activation of effector T cells in CLN. CD44 initiates T cell migration but is also involved in the interaction between T cells and APCs, which further promotes T cell activation (41). Reduced CD4$^+$ T cell activation in CLN is consistent with fewer CD4 T cells in the CNS, which may contribute to the inability of Ifit2$^{-/-}$ mice to combat RSA59 virus infection, even when the inoculating virus dose is lowered to 1/10th of the half of LD50 dose of RSA59.

In addition to impaired T cell priming, the integrity of the BBB may contribute to a paucity of lymphocyte accumulation in the absence of Ifit2. The BBB comprises capillary

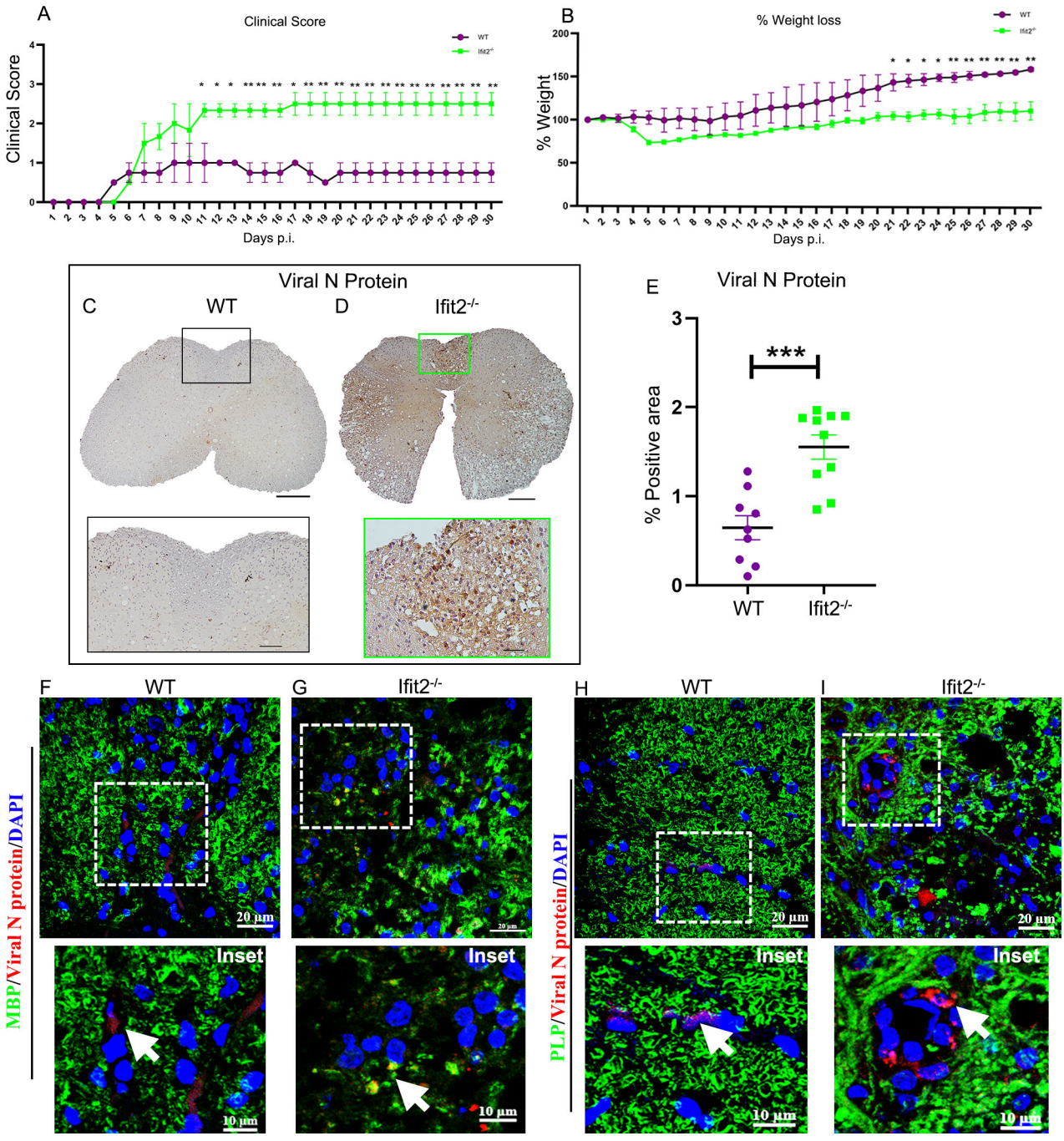

FIG 6 Ifit2$^{-/-}$ mice infected with low dose RSA59 showed severe weight loss, heightened clinical score, sustained viral persistence, and severe demyelination during persistent infection. 4–5-week-old WT and Ifit2$^{-/-}$ mice were infected intracranially with 20,000 or 500 PFU of RSA59, respectively, and monitored for development of clinical disease (A) and weight loss (B). Clinical scores were assigned by an arbitrary scale of 0–4 where an increasing score correlates with increased clinical impairment, as described in Materials and Methods. Purple color denotes WT and green color denotes Ifit2$^{-/-}$ mice. (C and D) Representative staining of spinal cord cross sections for viral antigen in WT and Ifit2$^{-/-}$ mice at day 30 p.i. using mouse anti-N antisera; corresponding enlarged regions are highlighted by black square for WT and green square for Ifit2$^{-/-}$ mice. The scale bar is 200 µm for spinal cord and 50 µm for the enlarged region. (E) Quantification of the presence of viral antigen in the spinal cord. (F–I) Representative immunofluorescence images of WT and Ifit2$^{-/-}$ spinal cord sections stained for MBP (green), viral antigen (red), and Dapi (blue) (F,G) or PLP (green), viral antigen (red) and Dapi (blue) (H and I); white arrows in enlarged sections show viral antigen in white matter region. The scale bar is 20 µm in spinal cord sections and 10 µm in enlarged insets. The experiment was repeated three times with $N = 4–5$ mice per experiment. Each dot in graph represents the average weight change of eight to nine mice. Asterix (*) indicates statistical significance by two-way ANOVA analysis for clinical score and percentage weight loss and Student's unpaired *t*-test analysis for viral N protein quantification (**$P < 0.01$, ***$P < 0.001$). The error bars represent SEM.

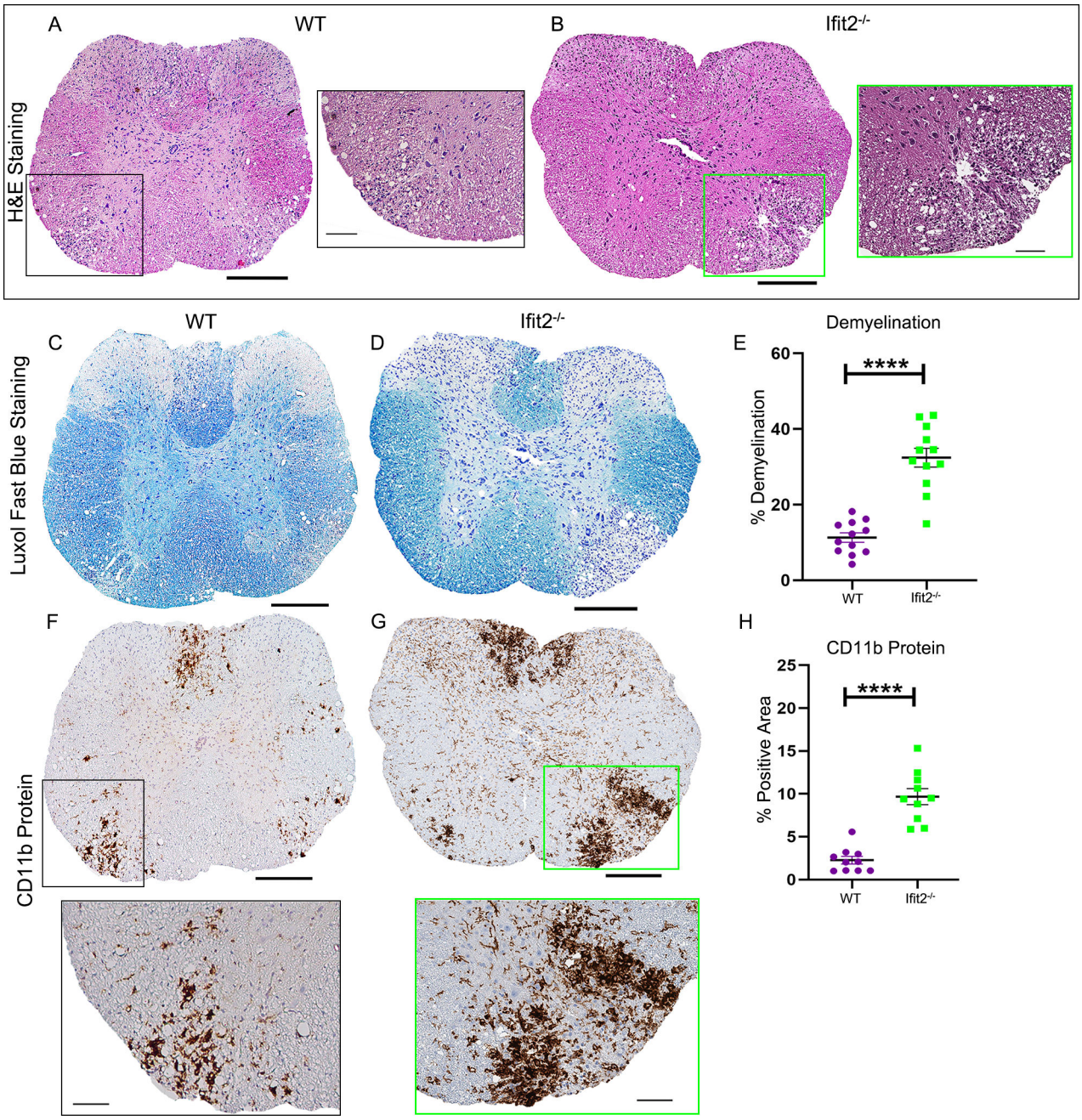

FIG 7 Ifit2 deficiency causes severe myelitis, chronic demyelination, and heightened accumulation of microglia/macrophages. Mice were infected, as described in Fig. 6 legend . Cross sections of WT and Ifit2$^{-/-}$ mouse spinal cords were analyzed for the presence of inflammatory lesions by H&E (A and B), demyelination by LFB (C and D), and CD11b^{+} myeloid cells (F and G). Corresponding enlarged regions are highlighted by the black square for WT and the green square for Ifit2$^{-/-}$ mice. (E and H) Quantification of white matter demyelination and myeloid cells by CD11b expression, respectively. The scale bar for spinal cord sections is 200 µm and 50 µm for the enlarged region. Statistical significance was calculated by unpaired Student's *t*-test and Welch correction (*$P < 0.05$, **$P < 0.01$, ****$P < 0.0001$). The data represent the results from four or five independent biological experiments with three to four mice each. Each dot represents a single animal. The error bars represent SEM

endothelial cells, astrocyte foot processes, and pericytes. The endothelial cells in the brain capillaries form tight cell-to-cell junctions composed of tight junction proteins such as claudins, which interact with ZO-1,2,3. The permeability of the BBB is compromised in injury from trauma, MS, HIV infection, brain tumor, or other noninfectious inflammatory processes (21, 22). Our data surprisingly revealed that the BBB integrity remained largely

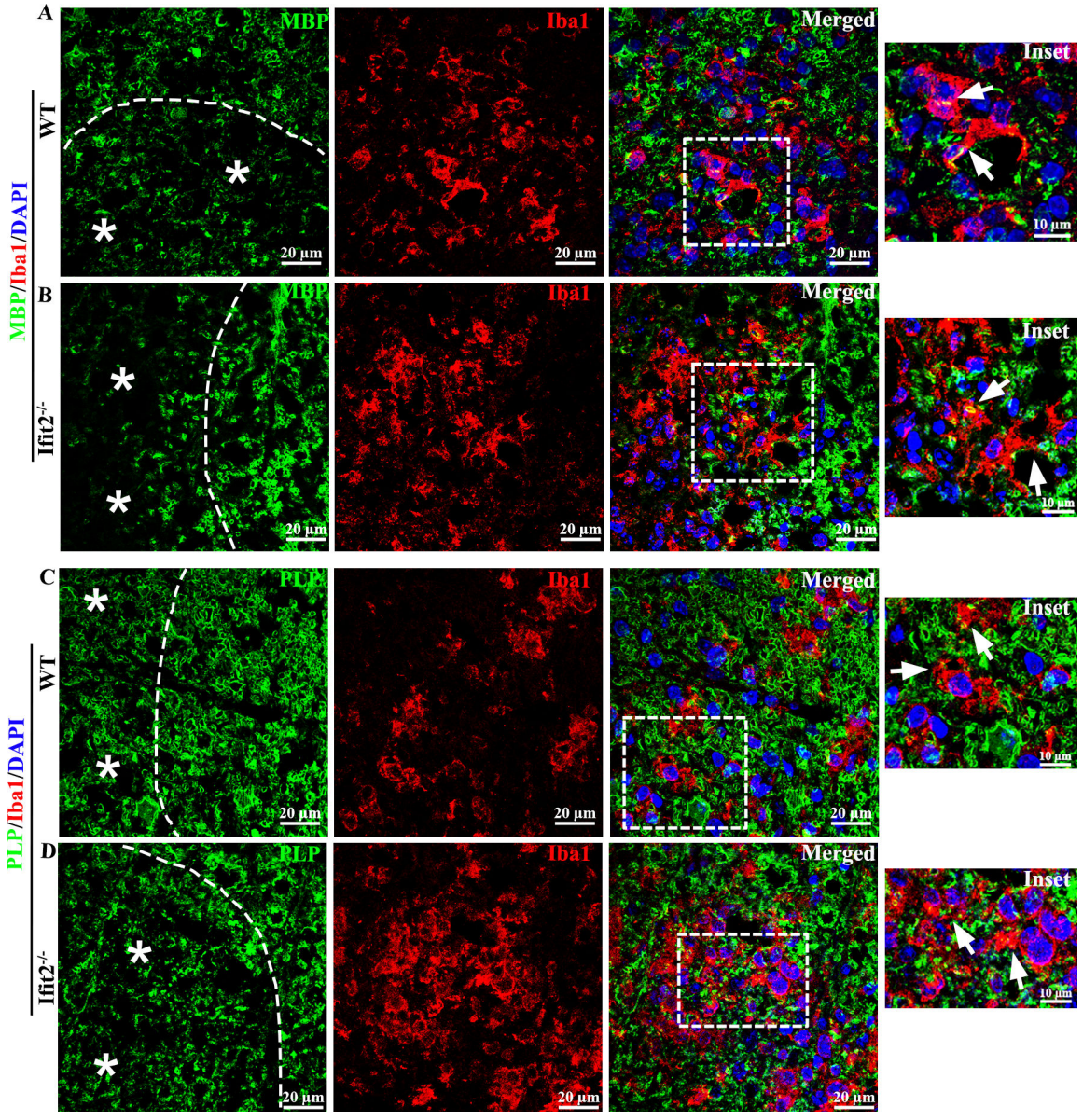

FIG 8 Ifit2 deficiency leads to enhanced engulfment of myelin by microglia/ macrophages. 5–10 µm thick paraffin sections were prepared from spinal cords of 4–5-week-old WT and Ifit2$^{-/-}$ RSA59-infected mice at day 30 p.i. Sections were stained for Iba1 (red), MBP and PLP (green), and nuclei using DAPI (blue). Representative images show areas of demyelination as indicated by loss of MBP (A and B) or PLP (C and D) together with Iba1 staining-activated microglia/macrophages. Demyelinating areas are demarcated by a white dotted line and highlighted by an asterisk. Boxed areas in merged images show areas of overlapping staining with Iba1 and MBP or PLP, respectively; white arrows inside the enlarged area insets indicate engulfment of myelin proteins by microglia/macrophages in both WT and Ifit2$^{-/-}$ mice. The scale bar for spinal cord sections is 20 µm and 10 µm for the enlarged region (inset).

intact in RSA59-infected Ifit2$^{-/-}$ compared to WT mice as observed by dye transfer assay and immunofluorescence analysis of ZO-1 and claudin-5 colocalization. Furthermore, mRNA expression of various cytokines and chemokines such as IFNα, IFNβ, IFNγ, IL-6, CCL2, CCL5, CSF2, CXCL9, CXCL10, and Nos2 that promotes key functions such as BBB destabilization, immune cells activation, cell migration, and recruitment of circulating immune cells remains largely unaltered in the CNS of Ifit2$^{-/-}$ compared to WT mice as opposed to CLN of Ifit2$^{-/-}$ mice despite extensive viral load in both the tissues (7, 17). A plausible explanation for this difference could be the presence of astrocytes in the CNS, which also secretes similar inflammatory chemokines/cytokines and compensate for some of the functional void caused by impaired activation of microglia/macrophages

and lymphocytes in the acute phase of neuroinflammation. The retention of BBB integrity, despite similar cytokine and chemokine mRNA expression in the CNS compared to WT mice advocates a key role of Ifit2 in regulating BBB permeability. Myosin II-dependent endocytosis of various tight junction proteins by blood vessel endothelial cells upon IFNγ secretion by circulating T cells may result in enhanced permeability of BBB (42). Furthermore, in several viral infections, IFNγ-expressing T cells are recruited to the site of infection by IFNγ-mediated stimulation of CXCL10 expression, in a feedforward mechanism. This causes the recruitment of more inflammatory cells to sites of infection thus producing inflammatory mediators that may impair BBB function. This IFNγ/CXCL10 axis is a major source of BBB breakdown and neuroinflammation during several CNS infections (43). In addition, CX3CR1, which is a transmembrane G-protein-coupled receptor expressed primarily on immune cells and known to interact with its unique ligand fractalkine/CX3CL1, also plays important role in determining BBB permeability. Endothelial cells through CX3CL1 can recruit the circulating peripheral immune cells, expressing CX3CR1, and promoting their migration to the infection site through the BBB (7, 44). The previous study showed a significant reduction in the expression of CX3CR1 in infiltrating peripheral immune cells and CNS resident microglia in the absence of Ifit2, indicating an impaired CX3CR1-CX3CL1 axis in Ifit2$^{-/-}$ mice (7). In our studies, we have observed significantly reduced expression of IFNγ in CD4^{+} T cells in CLN of Ifit2$^{-/-}$ mice. This reduced expression of IFNγ in Ifit2 deficiency could result in an impaired IFNγ/CXCL10 axis along with the previously established impaired CX3CR1-CX3CL1 axis. These can be some of the probable mechanisms for the Ifit2-dependent regulation of BBB permeability. Impaired T cell priming and an intact BBB may thus contribute to impaired virus control and exacerbated disease progression in Ifit2$^{-/-}$ mice.

Microglia are key players in maintaining CNS homeostasis (45). Our current study demonstrated that Ifit2 deficiency impaired the activation of microglia/macrophages in the spinal cord during the acute phase of RSA59-induced neuroinflammation, similar to findings in the brain where impaired microglial activation was accompanied by restricted expression of CX3CR1 on their surface, despite a substantially high viral load (7). However, these microglia/macrophages remained highly phagocytic in the spinal cords of Ifit2$^{-/-}$ mice at the chronic phase of the disease, presumably due to significantly elevated virus persistence potentially driving proinflammatory responses. Immunofluorescence staining in demyelinated areas of the spinal cord using myelin proteins MBP and PLP along with microglia/macrophage protein Iba1 confirmed the engulfment of myelin by phagocytic microglia/macrophages. Increased viral load associated with an increase in demyelinated areas containing highly activated microglia/macrophages in Ifit2$^{-/-}$ mice manifested are thus responsible for worsening disease manifested by partial to complete hind-limb paralysis and ultimately leading to a moribund state and death.

In conclusion, our study identifies a role for Ifit2 in promoting inflammation during the acute phase of viral infection by promoting activation of T cells in the CLN, triggering BBB permeability, and promoting leukocyte infiltration into the CNS. The lack of functional Ifit2 may result in microglial cells' inability to initiate and promote neuroinflammation, thereby impairing viral control in the acute phase resulting in viral persistence and aggravated demyelinating disease in the chronic phase. Our results thus revealed pleiotropic effects of Ifit2 in both immune activation and effector sites, and support protective function in various diseases, including the autoimmune-mediated model of demyelination of experimental allergic encephalomyelitis (46). It is thus important to understand the contribution of cell-specific Ifit2 functions in various disease models.

MATERIALS AND METHODS

Virus infection in mice

MHV-free C57BL/6 mice and homozygous Ifit2$^{-/-}$ mice on the C57BL/6 background bred at the breeding colony of LRI Biological Resources Unit, Lerner Research Institute, Cleveland

Clinic, USA, as previously described (7). All animal experiments were carried out in strict accordance with all provisions of the Animal Welfare Act, the Guide for the Care and Use of Laboratory Animals, and the PHS Policy on Humane Care and Use of Laboratory Animals. All animal experiments were performed in compliance with protocols approved by the Cleveland Clinic Institutional Animal Care and Use Committee (PHS assurance number A3047-01). All mice were housed under pathogen-free conditions at an accredited facility at the Cleveland Clinic Lerner Research Institute and used at 4–5 weeks of age. The hepatotropic and neurotropic recombinant, EGFP-expressing strain of MHV-A59 known as RSA59 was used in the study (9). The virus was propagated in 17Cl1 cells and plaque assayed on DBT astrocytoma cell monolayers (11). Male mice were infected intracranially in the right hemisphere with 500 PFU and 2000 PFU for Ifit2$^{-/-}$ mice and 2,000 and 20,000 PFU for WT mice of RSA59 diluted in endotoxin-free, filter-sterilized phosphate-buffered saline (PBS)–bovine serum albumin (BSA) (Dulbecco's PBS +0.75% BSA) in a final volume of 20 µL. Age-matched mice were mock-infected with PBS-BSA or not infected and kept as noninfected control. Clinical disease severity was graded daily using the following scale as discussed (7, 10): 0, no disease symptoms; 1, ruffled fur; 1.5, hunched back with mild ataxia; 2, ataxia, balance problem, and hind limb weakness; 2.5, one leg completely paralyzed, motility issue but still able to move around with difficulties; 3, severe hunching/wasting/both hind limb paralysis and mobility is severely compromised; 3.5, severe distress, complete paralysis, and moribund; 4, dead. Our study also investigated for any phenotypic or pathological symptoms between age-matched control (noninfected) and mock-infected WT and Ifit2$^{-/-}$ male mice, but no such significant gross phenotypic clinical symptoms or histological changes were observed.

Histopathological and immunohistochemical analysis

Hematoxylin/eosin staining

RSA59-infected mice from C57BL/6 WT and Ifit2$^{-/-}$ groups were sacrificed at day 5 p.i. and day 30 p.i., and were perfused transcardially with PBS followed by PBS containing 4% paraformaldehyde (PFA). All spinal cords were collected, post-fixed in 4% PFA overnight, and embedded in paraffin. Tissues were sectioned at 5 µm and stained with hematoxylin/eosin (H&E) to evaluate inflammation (16). Experiments were repeated four times with three to four mice in each group.

Luxol fast blue staining

Mice were sacrificed at day 30 p.i. Following transcardial perfusion with PBS and 4% PFA, spinal cords were harvested and embedded in paraffin. 5 µm thick sections of the embedded tissues were prepared and stained with Luxol fast blue (LFB) stain to evaluate demyelination in the spinal cord tissues, as described previously with minor modifications (13, 20). Experiments were repeated four times with three to four mice in each group.

Immunohistochemical staining and quantification

Serial sections from the spinal cord were stained by the avidin–biotin–immunoperoxidase technique (Vector Laboratories) using 3, 3′-diaminobenzidine as substrate, and anti-Iba1 (Wako, 1:250), CD11b (ABclonal, 1:250), anti-GFAP (Sigma, 1:500), and anti-N (kind gift from Julian Leibowitz, Texas A&M University) (1:50), as primary antibodies. Control slides from mock-infected or uninfected mice were incubated in parallel. Seven to eight sections from each infected group were randomly selected from three different sets of experiments, and the expression of viral antigen, GFAP and Iba1 was quantified. Briefly, whole slides were scanned in a Leica Aperio AT2 slide scanner (Leica Microsystems, GmbH, Wetzlar, Germany) at ×20 magnification and analyzed in Aperio Imagescope version 10.0.36.1805 software (Aperio) and quantified. For quantification, brightfield images of spinal cord sections were analyzed using open-source software

QuPath (47). Experiments were repeated four times with three to four mice in each group. Whole tissue sections were selected as regions of interest for analysis. Areas with tissue folding, damage, or out-of-focus tissue were then excluded by manual annotation. Stain colors were separated into respective components by RGB-dependent color deconvolution. The positive pixel area was then measured as a percentage using thresholding on the deconvolved stained images.

Immunofluorescence microscopy

Infected WT and Ifit2$^{-/-}$ mice were sacrificed at day 5 and day 30 p.i. and spinal cord tissue sections were harvested, processed, and embedded in paraffin. 5 µm thick transverse sections of spinal cord were used to perform immunofluorescence imaging. The tissue sections used were parallel to those used for the corresponding histopathology. Briefly, the slides were deparaffinized followed by rehydration and antigen unmasking. The slides were then permeabilized with 0.2% Triton X-100 in PBS by shaking incubation at RT for 15 min and blocked using 1% BSA prepared in 0.2% Triton X-100–1X PBS solution at 37°C for 1 h. This was followed by shaking incubation at 4°C for 16 h with primary antibodies prepared in blocking solution. Each section on each sample slide was stained for the following combinations separately: (i) rabbit anti-Iba1 (1: 500, Wako; Catalog No. 019–19741) and anti-MBP homemade serum antibody raised in rat (1:1); (ii) rabbit anti-Iba1 (1:500) and homemade serum antibody against PLP raised in rat (1:1); (iii) mouse anti-N (1:40) and homemade serum antibody against PLP raised in rat (1:1); (iv) anti-N (1:40) and homemade serum antibody against MBP (1:1). Slides were then washed and incubated for 1 h at 37°C with a combination of secondary antibodies Alexa Fluor 568 (donkey anti rabbit, Invitrogen, A10042) and Alexa Fluor 488 (goat anti mouse, Invitrogen, A11001), Alexa Fluor 488 (goat anti rat, Invitrogen, A-11006) (1:750 each) prepared in blocking solution. Finally, the slides were washed in PBS and mounted using Vectashield with DAPI. Confocal imaging was performed using Zeiss confocal microscope (LSM710) were processed with Zen 2010 software.

Gene expression: RNA isolation, reverse transcription, and quantitative polymerase chain reaction

RNA was extracted from the brain or CLN (flash-frozen) of RSA59-infected WT and Ifit2$^{-/-}$ mice using the Trizol isolation protocol following transcardial perfusion with 1X PBS. The total RNA concentration was measured using a NanoDrop ND-2000 spectrophotometer. 1 µg of RNA was used to prepare cDNA using a High-Capacity cDNA Reverse Transcription Kit (Applied Biosystems). Quantitative real-time PCR analysis was performed using DyNAmo Color Flash SYBR Green qPCR kit (Thermo Scientific) in a StepOnePlus Real-time PCR system (Thermo Fisher Scientific) under the following conditions: initial denaturation at 95°C for 7 min, 40 cycles of 95°C for 10 s, 60°C for 30 s, melting curve analysis at 60°C for 30 s. All samples were run in quadruplicates on a 96-well plate with an automatically set baseline and a manually set critical threshold (CT) at which the fluorescent signal becomes higher than the signals for all of the PCR pairs. Dissociation curves were used to confirm amplification of a single product for each primer pair per sample. Primer sequences are mentioned in Table 1.

BBB analysis

RSA59-infected mice from both C57BL/6 WT and Ifit2$^{-/-}$ groups were sacrificed at day 5 p.i. and were perfused transcardially with PBS followed by PBS containing 4% PFA. Whole brains were collected, post-fixed in 4% PFA overnight, and embedded in paraffin. Tissues were sectioned at 5 µm and stained by rabbit anti ZO-1 (Invitrogen, 1:100) and mouse anti-claudin 5 (Invitrogen 1:50) as primary antibody and Alexa Fluor 568 (donkey anti rabbit, Invitrogen, A10042) and Alexa Fluor 488 (goat anti mouse, Invitrogen, A11001) as described (48). For dye transmigration assay, mice were injected with 100 µL per mouse of 10 mM of Texas red dextran intraperitonially and intravenously. 15 min after

TABLE 1 List of primers

GENE	Primer (5′–3′)
18S	FP: GGGAGCCTGAGAAACGGC
	RP: GGGTCGGGAGTGGGTAATTT
VIRAL	FP: GTTGCAAACAGCCAAGCG
N gene	RP: GGGCGCAAACCTAGT
Ifn γ	FP: ATCTGGAGGAACTGGCAAAA
	RP: TTCAAGACTTCAAAGAGTCTGAGG
Ifn α	FP: CTTCCACAGGATCACTGTGTACCT
	RP: TTCTGCTCTGACCACCTCCC
Ifn β	FP: CTGGCTTCCATCATGAACAA
	RP: AGAGGGCTGTGGTGGAGAA
Tnf α	FP: GGTCTGGGCCATAGAACTGATG
	RP: AGCAGGTGTCCCAAAGAA
Cxcl9	FP: CTTTTCCTCTTGGGCATCAT
	RP: GCATCGTGCATTCCTTATCA
Csf2	FP: GCATGTAGAGGCCATCAAAGA
	RP: CGGGTCTGCACACATGTTA
CD4	FP: CTGACTCTGACTCTGGACAA
	RP: TGAGCTGAGCCACTTTC
CD8	FP: TACTTCTGCGCGACGGTT
	RP: GCAGTTGTAGGAAGGACATC
IL-1 beta	FP: TGTAATGAAAGACGGCACACC
	RP: TCTTCTTTGGGTATTGCTTGG
CD40	FP: AGGAACGAGTCAGACTAATGT
	RP: GGATCTTGCCGTCGAGC

injection, mice were anesthetized with an intraperitoneal (I.P.) injection of ketamine and xylazine (100 mg and 5–10 mg in 0.9% saline per kg body weight, respectively, 150 µL of the cocktail per 25 g mouse weight), followed by transcardial perfusion with PBS. The brain tissue was then harvested and homogenized. After centrifugation of the samples at 10,000 g for 15 min at 4◦C, the supernatant was measured to obtain raw fluorescence units in a fluorescence plate reader at excitation/emission wavelength of 595/625 nm (23). Experiments were repeated four times with three to four mice in each group. Fluorescence was plotted between mock-infected WT and Ifit2$^{-/-}$ mice and RSA59-infected WT and Ifit2$^{-/-}$ mice in graphs after subtraction from autofluorescence values.

Flow cytometry analysis

Mice were perfused with PBS, and the spinal cords were homogenized in 4 mL of Dulbecco's PBS (pH 7.4) using Tenbroeck tissue homogenizers. Following centrifugation at 450 g for 10 min, cell pellets were resuspended in RPMI containing 25 mM HEPES (pH 7.2), adjusted to 30% Percoll (Sigma), and underlaid with 1 mL of 70% Percoll. Following centrifugation at 800 g for 30 min at 4°C, cells were recovered from the 30%–70% interface, washed with RPMI, and suspended in FACS buffer (0.5% BSA in Dulbecco's PBS). Also, deep CLNs were harvested, homogenized in 4 mL RPMI containing 25 mM HEPES (pH 7.2), and passed through 70 µm filters followed by 30 µm filters to obtain single-cell suspensions. Following centrifugation at 45 g for 10 min, cell pellets were resuspended in FACS buffer. For intracellular staining, CNS-derived cells were stimulated for 6 h with phorbol 12-myristate 13-acetate (PMA) (10 ng/ml) (Acros Organics, Geel, Belgium) and ionomycin (1 µM) (Calbiochem, Spring Valley, CA, USA), with Monensin (2 µM) (Calbiochem) added for the last 2 h. Following stimulation, surface molecules were detected as described subsequently. Cells were permeabilized using cytofix/cytoperm solution (BD Biosciences, San Jose, CA, USA) and incubated for 30 min on ice with fluorescent

monoclonal antibody (mAb) specific for IFN-γ (XMG1.2; BD Biosciences). Cells were then washed using perm/wash buffer according to the manufacturer's instructions (49). Cells were counted using an automated cell counter (Invitrogen) to obtain the number of total leukocytes. One million cells were stained for flow cytometry (7, 20). Fc receptors were blocked with 1% polyclonal mouse serum and 1% rat anti-mouse CD16/CD32 (clone 2.4G2; BD Biosciences) monoclonal antibody (MAb) for 20 min. Specific cell types were identified by staining with fluorescein isothiocyanate-, phycoerythrin (PE)-, peridinin chlorophyll protein (PerCP)-, or allophycocyanin (APC)-conjugated MAb for 30 min on ice in FACS buffer. Expression of surface markers was characterized with MAb (all from BD Biosciences except where otherwise indicated) specific for CD45 (clone Ly-5), CD4 (clone GK1.5), CD8 (clone 53–6.7), CD11b (clone M1/70), Ly-6G (clone 1A8), NK1.1 (clone PK136), CD44 (clone IM7), CD62L (MEL-14), and IFNγ (clone XMG1.2). Samples were analyzed using a BD LSRFortesa flow cytometer (BD Biosciences) and FlowJo 10 software (Treestar, Inc., Ashland, OR, USA). First, doublet exclusion using FSC-A and FSC-W was performed, and then cells were gated based on forward scatter (FSC) and side scatter (SSC) to focus on live cells. Cells were gated from a primary gating on CD45. Single colors and FMOs were used in all the experiments.

Statistical analysis

All immunohistochemical analysis and flow cytometry statistical analysis was performed by Student's unpaired *t*-test. Data were analyzed using Prism software (GraphPad Prism 8). Two-way ANOVA analysis for clinical score and weight loss (*$P < 0.05$,**$P < 0.01$, ***$P < 0.001$, ****$P < 0.0001$).

ACKNOWLEDGMENTS

We thank the Lerner Research Institute, Cleveland Clinic where all the experiments were done. We thank the LRI Biological Resources Unit for assistance with animal care and handling. The authors also thank the members of the LRI Imaging Core: Diane Mahovlic and Andrelie Branicky for histology services, Kelly Simmerman for immunohistochemistry, Dr. Gauravi Deshpande for help with imaging and analyses, and Dr. Judy Drazba for project consultation. We thank CSIR for providing fellowship to MS, IISER-Kolkata for providing fellowship to DC. We thank IISER-Kolkata Central Imaging Facility for image acquisition. We also want to thank SERB-POWER (Promoting Opportunities for Women in Exploratory Research) program for providing research funds to JDS for structured effort toward enhanced diversity in research to ensure equal access and weighted opportunities for Indian women scientists engaged in research and development activities.

This work was supported by the National Institutes of Health grant: R01-CA068782, Antiviral actions of Interferons to GS and SERB-POWER grant: SPG/2020/000454 (Promoting Opportunities for Women in Exploratory Research) program for research funds to JDS. The funders had no role in study design, data collection and analysis, decision to publish, or preparation of the manuscript.

The authors have declared that no competing interests exist.

Conceptualization: Jayasri Das Sarma; Data curation: Madhav Sharma, Debanjana Chakravarty, Amy Burrows, Patricia Rayman, Jayasri Das Sarma; Formal analysis: Madhav Sharma, Debanjana Chakravarty, Afaq Hussain, Ajay Zalavadia, Nikhil Sharma, Amy Burrows, Patricia Rayman, Jayasri Das Sarma; Funding acquisition: Jayasri Das Sarma, Ganes C. Sen; Investigation: Jayasri Das Sarma; Methodology: Madhav Sharma, Debanjana Chakravarty, Afaq Hussain, Amy Burrows, Patricia Rayman, Jayasri Das Sarma; Project administration: Jayasri Das Sarma; Resources: Jayasri Das Sarma, Ganes C. Sen; Software: Madhav Sharma, Debanjana Chakravarty, Ajay Zalavadia, Jayasri Das Sarma; Supervision: Jayasri Das Sarma, Cornelia Bergmann, Ganes C. Sen; Validation: Jayasri Das Sarma, Cornelia Bergmann, Ganes C. Sen; Visualization: Jayasri Das Sarma; Writing—original draft: Madhav Sharma, Debanjana Chakravarty, Jayasri Das Sarma; Writing—

review & editing: Jayasri Das Sarma, Lawrence C. Kenyon, Cornelia Bergmann, Ganes C. Sen.

AUTHOR AFFILIATIONS

[1]Department of Biological Sciences, Indian Institute of Science Education and Research Kolkata, Mohanpur, West Bengal, India
[2]Department of Inflammation and Immunity, Lerner Research Institute, Cleveland Clinic, Cleveland, Ohio, USA
[3]Department of Pathology, Anatomy and Cell Biology, Thomas Jefferson University, Philadelphia, Pennsylvania, USA
[4]Department of Neurosciences, Cleveland Clinic, Cleveland, Ohio, USA

AUTHOR ORCIDs

Jayasri Das Sarma http://orcid.org/0000-0002-3980-4060

FUNDING

Funder	Grant(s)	Author(s)
HHS | National Institutes of Health (NIH)	R01-CA068782	Ganes C Sen
DST | Science and Engineering Research Board (SERB)	SPG/2020/000454	Jayasri Das Sarma
CSIR | Human Resource Development Group (HRDG)		Madhav Sharma
Indian Institute of Science Education and Research Kolkata (IISER-K)		Debanjana Chakravarty

AUTHOR CONTRIBUTIONS

Madhav Sharma, Data curation, Formal analysis, Methodology, Software, Writing – original draft | Debanjana Chakravarty, Data curation, Formal analysis, Methodology, Software, Writing – original draft | Afaq Hussain, Formal analysis, Methodology, Software | Ajay Zalavadia, Formal analysis, Software | Amy Burrows, Data curation, Formal analysis, Methodology | Patricia Rayman, Data curation, Formal analysis, Methodology | Nikhil Sharma, Formal analysis | Lawrence C Kenyon, Writing – review and editing | Cornelia Bergmann, Supervision, Validation, Writing – review and editing | Ganes C. Sen, Funding acquisition, Resources, Supervision, Validation, Writing – review and editing | Jayasri Das Sarma, Conceptualization, Data curation, Formal analysis, Funding acquisition, Investigation, Methodology, Project administration, Resources, Software, Supervision, Validation, Visualization, Writing – original draft, Writing – review and editing

REFERENCES

1. Das Sarma J. 2010. A mechanism of virus-induced demyelination. Interdiscip Perspect Infect Dis 2010:109239. https://doi.org/10.1155/2010/109239
2. Dobson R, Giovannoni G. 2019. Multiple sclerosis - a review. Eur J Neurol 26:27–40. https://doi.org/10.1111/ene.13819
3. Feng X, Petraglia AL, Chen M, Byskosh PV, Boos MD, Reder AT. 2002. Low expression of interferon-stimulated genes in active multiple sclerosis is linked to subnormal phosphorylation of STAT1. J Neuroimmunol 129:205–215. https://doi.org/10.1016/s0165-5728(02)00182-0
4. Findling O, Sellner J. 2021. Second-generation immunotherapeutics in multiple sclerosis: can we discard their precursors Drug Discov Today 26:416–428. https://doi.org/10.1016/j.drudis.2020.11.022
5. Fensterl V, Chattopadhyay S, Sen GC. 2015. No love lost between viruses and interferons. Annu Rev Virol 2:549–572. https://doi.org/10.1146/annurev-virology-100114-055249
6. Fensterl V, Sen GC. 2015. Interferon-induced Ifit proteins: their role in viral pathogenesis. J Virol 89:2462–2468. https://doi.org/10.1128/JVI.02744-14
7. Das Sarma J, Burrows A, Rayman P, Hwang MH, Kundu S, Sharma N, Bergmann C, Sen GC. 2020. IFIT2 deficiency restricts microglial activation and leukocyte migration following murine coronavirus (M-Cov) CNS infection. PLoS Pathog 16:e1009034. https://doi.org/10.1371/journal.ppat.1009034
8. Perlman S, Sun N, Barnett EM. 1995. Spread of MHV-JHM from nasal cavity to white matter of spinal cord. Transneuronal movement and involvement of astrocytes. Adv Exp Med Biol 380:73-8.
9. Sarma JD, Scheen E, Seo S-H, Koval M, Weiss SR. 2002. Enhanced green fluorescent protein expression may be used to monitor murine coronavirus spread *in vitro* and in the mouse central nervous system. J Neurovirol 8:381–391. https://doi.org/10.1080/13550280260422686
10. Singh M, Khan RS, Dine K, Das Sarma J, Shindler KS. 2018. Intracranial inoculation is more potent than intranasal inoculation for inducing optic

neuritis in the Mouse hepatitis virus-induced model of multiple sclerosis. Front Cell Infect Microbiol 8:311. https://doi.org/10.3389/fcimb.2018.00311
11. Singh M, Kishore A, Maity D, Sunanda P, Krishnarjuna B, Vappala S, Raghothama S, Kenyon LC, Pal D, Das Sarma J. 2019. A proline insertion-deletion in the spike glycoprotein fusion peptide of mouse hepatitis virus strongly alters neuropathology. J Biol Chem 294:8064–8087. https://doi.org/10.1074/jbc.RA118.004418
12. Kishore A, Kanaujia A, Nag S, Rostami AM, Kenyon LC, Shindler KS, Das Sarma J. 2013. Different mechanisms of inflammation induced in virus and autoimmune-mediated models of multiple sclerosis in C57Bl6 mice. Biomed Res Int 2013:589048. https://doi.org/10.1155/2013/589048
13. Das Sarma J, Kenyon LC, Hingley ST, Shindler KS. 2009. Mechanisms of primary axonal damage in a viral model of multiple sclerosis. J Neurosci 29:10272–10280. https://doi.org/10.1523/JNEUROSCI.1975-09.2009
14. Chatterjee D, Addya S, Khan RS, Kenyon LC, Choe A, Cohrs RJ, Shindler KS, Sarma JD. 2014. Mouse hepatitis virus infection upregulates genes involved in innate immune responses. PLoS One 9:e111351. https://doi.org/10.1371/journal.pone.0111351
15. Biswas K, Chatterjee D, Addya S, Khan RS, Kenyon LC, Choe A, Cohrs RJ, Shindler KS, Das Sarma J. 2016. Demyelinating strain of mouse hepatitis virus infection bridging innate and adaptive immune response in the induction of demyelination. Clin Immunol 170:9–19. https://doi.org/10.1016/j.clim.2016.07.004
16. Chakravarty D, Saadi F, Kundu S, Bose A, Khan R, Dine K, Kenyon LC, Shindler KS, Das Sarma J. 2020. CD4 deficiency causes poliomyelitis and axonal blebbing in murine coronavirus-induced neuroinflammation. J Virol 94:e00548-20. https://doi.org/10.1128/JVI.00548-20
17. Butchi NB, Hinton DR, Stohlman SA, Kapil P, Fensterl V, Sen GC, Bergmann CC. 2014. IFIT2 deficiency results in uncontrolled neurotropic coronavirus replication and enhanced encephalitis via impaired alpha/beta interferon induction in macrophages. J Virol 88:1051–1064. https://doi.org/10.1128/JVI.02272-13
18. Catron DM, Rusch LK, Hataye J, Itano AA, Jenkins MK. 2006. CD4+ T cells that enter the draining lymph nodes after antigen injection participate in the primary response and become central-memory cells. J Exp Med 203:1045–1054. https://doi.org/10.1084/jem.20051954
19. Kak G, Raza M, Tiwari BK. 2018. Interferon-gamma (IFN-gamma): exploring its implications in infectious diseases. Biomol Concepts 9:64–79. https://doi.org/10.1515/bmc-2018-0007
20. Saadi F, Chakravarty D, Kumar S, Kamble M, Saha B, Shindler KS, Das Sarma J. 2021. CD40L protects against Mouse hepatitis virus-induced neuroinflammatory demyelination. PLoS Pathog 17:e1010059. https://doi.org/10.1371/journal.ppat.1010059
21. Al-Obaidi MMJ, Bahadoran A, Wang SM, Manikam R, Raju CS, Sekaran SD. 2018. Disruption of the blood brain barrier is vital property of neurotropic viral infection of the central nervous system. Acta Virol 62:16–27. https://doi.org/10.4149/av_2018_102
22. Abbott NJ, Patabendige AAK, Dolman DEM, Yusof SR, Begley DJ. 2010. Structure and function of the blood-brain barrier. Neurobiology of Disease 37:13–25. https://doi.org/10.1016/j.nbd.2009.07.030
23. Scalisi J, Balau B, Deneyer L, Bouchat J, Gilloteaux J, Nicaise C. 2021. Blood-brain barrier permeability towards small and large tracers in a mouse model of osmotic demyelination syndrome. Neurosci Lett 746:135665. https://doi.org/10.1016/j.neulet.2021.135665
24. Luissint AC, Artus C, Glacial F, Ganeshamoorthy K, Couraud PO. 2012. Tight Junctions at the blood brain barrier: physiological architecture and disease-associated dysregulation. Fluids Barriers CNS 9:23. https://doi.org/10.1186/2045-8118-9-23
25. Jurga AM, Paleczna M, Kuter KZ. 2020. Overview of general and discriminating markers of differential microglia phenotypes. Front Cell Neurosci 14:198. https://doi.org/10.3389/fncel.2020.00198
26. Butts BD, Houde C, Mehmet H. 2008. Maturation-dependent sensitivity of oligodendrocyte lineage cells to apoptosis: implications for normal development and disease. Cell Death Differ 15:1178–1186. https://doi.org/10.1038/cdd.2008.70
27. Yang Z, Liang H, Zhou Q, Li Y, Chen H, Ye W, Chen D, Fleming J, Shu H, Liu Y. 2012. Crystal structure of ISG54 reveals a novel RNA binding structure and potential functional mechanisms. Cell Res 22:1328–1338. https://doi.org/10.1038/cr.2012.111
28. Sen GC, Fensterl V. 2012. Crystal structure of Ifit2 (ISG54) predicts functional properties of Ifits. Cell Res 22:1407–1409. https://doi.org/10.1038/cr.2012.130
29. Zhou Q, Li Y, Chen L, Zheng X, Jiang T, Liu J, Fu Y, Guan L, Ju J, Wu C. 2021. Long non-coding RNA GRIK1-AS1 inhibits the proliferation and invasion of gastric cancer cells by regulating the miR-375/IFIT2 axis. Front. Oncol 11:754834. https://doi.org/10.3389/fonc.2021.754834
30. Lai KC, Liu CJ, Chang KW, Lee TC. 2013. Depleting IFIT2 mediates atypical PKC signaling to enhance the migration and metastatic activity of oral squamous cell carcinoma cells. Oncogene 32:3686–3697. https://doi.org/10.1038/onc.2012.384
31. Fleith RC, Mears HV, Leong XY, Sanford TJ, Emmott E, Graham SC, Mansur DS, Sweeney TR. 2018. IFIT3 and IFIT2/3 promote IFIT1-mediated translation inhibition by enhancing binding to non-self RNA. Nucleic Acids Res 46:5269–5285. https://doi.org/10.1093/nar/gky191
32. Diamond MS, Farzan M. 2013. The broad-spectrum antiviral functions of IFIT and IFITM proteins. Nat Rev Immunol 13:46–57. https://doi.org/10.1038/nri3344
33. Chen L, Zhai W, Zheng X, Xie Q, Zhou Q, Tao M, Zhu Y, Wu C, Jiang J. 2018. Decreased IFIT2 expression promotes gastric cancer progression and predicts poor prognosis of the patients. Cell Physiol Biochem 45:15–25. https://doi.org/10.1159/000486219
34. Chen L, Liu S, Xu F, Kong Y, Wan L, Zhang Y, Zhang Z. 2017. Inhibition of proteasome activity induces aggregation of IFIT2 in the centrosome and enhances IFIT2-induced cell apoptosis. Int J Biol Sci 13:383–390. https://doi.org/10.7150/ijbs.17236
35. Chen H, Zheng J, Yan L, Zhou X, Jiang P, Yan F. 2021. Super-enhancer-associated long noncoding RNA Rp11-569A11.1 inhibited cell progression and metastasis by regulating IFIT2 in colorectal cancer. J Clin Lab Anal 35. https://doi.org/10.1002/jcla.23780
36. Saha S, Sugumar P, Bhandari P, Rangarajan PN. 2006. Identification of Japanese encephalitis virus-inducible genes in mouse brain and characterization of GARG39/IFIT2 as a microtubule-associated protein. J Gen Virol 87:3285–3289. https://doi.org/10.1099/vir.0.82107-0
37. Spindler KR, Hsu TH. 2012. Viral disruption of the blood-brain barrier. Trends Microbiol 20:282–290. https://doi.org/10.1016/j.tim.2012.03.009
38. de Vos AF, van Meurs M, Brok HP, Boven LA, Hintzen RQ, van der Valk P, Ravid R, Rensing S, Boon L, 't Hart BA, Laman JD. 2002. Transfer of central nervous system autoantigens and presentation in secondary lymphoid organs. J Immunol 169:5415–5423. https://doi.org/10.4049/jimmunol.169.10.5415
39. Sonar SA, Lal G. 2017. Differentiation and transmigration of CD4 T cells in neuroinflammation and autoimmunity. Front Immunol 8:1695. https://doi.org/10.3389/fimmu.2017.01695
40. Savarin C, Bergmann CC. 2018. Fine tuning the cytokine storm by IFN and IL-10 following neurotropic coronavirus encephalomyelitis. Front Immunol 9:3022. https://doi.org/10.3389/fimmu.2018.03022
41. Baaten BJ, Li CR, Bradley LM. 2010. Multifaceted regulation of T cells by CD44. Commun Integr Biol 3:508–512. https://doi.org/10.4161/cib.3.6.13495
42. Utech M, Ivanov AI, Samarin SN, Bruewer M, Turner JR, Mrsny RJ, Parkos CA, Nusrat A. 2005. Mechanism of IFN-gamma-induced endocytosis of tight junction proteins: myosin II-dependent vacuolarization of the apical plasma membrane. MBoC 16:5040–5052. https://doi.org/10.1091/mbc.e05-03-0193
43. Chai Q, He WQ, Zhou M, Lu H, Fu ZF. 2014. Enhancement of blood-brain barrier permeability and reduction of tight junction protein expression are modulated by chemokines/cytokines induced by rabies virus infection. J Virol 88:4698–4710. https://doi.org/10.1128/JVI.03149-13
44. Lee M, Lee Y, Song J, Lee J, Chang SY. 2018. Tissue-specific role of CX3CR1 expressing immune cells and their relationships with human disease. Immune Netw 18:e5. https://doi.org/10.4110/in.2018.18.e5
45. Shemer A, Erny D, Jung S, Prinz M. 2015. Microglia plasticity during health and disease: an immunological perspective. Trends Immunol 36:614–624. https://doi.org/10.1016/j.it.2015.08.003
46. Kim D, Rai NK, Burrows A, Kim S, Tripathi A, Weinberg SE, Dutta R, Sen GC, Min B. 2023. IFN-induced protein with tetratricopeptide repeats 2 limits autoimmune inflammation by regulating myeloid cell activation and metabolic activity. J Immunol 210:721–731. https://doi.org/10.4049/jimmunol.2200746

47. Bankhead P, Loughrey MB, Fernández JA, Dombrowski Y, McArt DG, Dunne PD, McQuaid S, Gray RT, Murray LJ, Coleman HG, James JA, Salto-Tellez M, Hamilton PW. 2017. Qupath: open source software for digital pathology image analysis. Sci Rep 7:16878. https://doi.org/10.1038/s41598-017-17204-5
48. Basu R, Banerjee K, Bose A, Das Sarma J. 2015. Mouse hepatitis virus infection remodels connexin43-mediated gap junction Intercellular communication *in vitro* and *in vivo*. J Virol 90:2586–2599. https://doi.org/10.1128/JVI.02420-15
49. Savarin C, Hinton DR, Valentin-Torres A, Chen Z, Trapp BD, Bergmann CC, Stohlman SA. 2015. Astrocyte response to IFN-gamma limits IL-6-mediated microglia activation and progressive autoimmune encephalomyelitis. J Neuroinflammation 12:79. https://doi.org/10.1186/s12974-015-0293-9